MODEL BASED AERO-STRUCTURAL DESIGN AND OPTIMIZATION OF A HIGHLY FLEXIBLE HIGH ASPECT-RATIO WING

H. Shahi*, P. J. González†, W. R. Krüger *, F. J. Silvestre†

* Department of Loads Analysis and Aeroelastic Design, Institute of Aeroelasticity, DLR German Aerospace Center, Göttingen, Germany

† Department of Flight Mechanics, Flight Control and Aeroelasticity, ILR, Technical University of Berlin (TUB), Berlin, Germany

Abstract

This research presents the model-based aerostructural design process of the highly flexible composite wing and its optimization process. The parametric modeling of the wing was carried out using DLR's ModGen, which generates all the essential features of the FE and Aero models of the wing. The models obtained are then integrated into the model-based design optimization framework, which seeks to minimize wing structural mass while maximizing structural flexibility with lower frequencies. This aligns with the core objective of the TU-Flex design, which is to develop a flying demonstrator with a wing bending frequency low enough to induce coupling with flight mechanics. Therefore, the spars of the Highly Flexible High Aspect-Ratio Wing are designed as the primary load-bearing structure, with minimal upper and lower skin thicknesses to minimize the wing bending frequency. The model-based design and optimization of the composite Wingbox is accomplished using a gradient-based optimization algorithm, with MSC Nastran.
Three maneuvers (1g, 4g and -2g) as well as two gust cases (positive and negative) are considered to determine the optimal Wingbox design. The structural mass, the thickness distribution on the semi-span, the effectiveness of the control surface, and the elastic characteristics of the wing are derived from the structural optimization of the composite wing. The optimized wing shows a deformation of 8.9% under a 1g flight condition, while still meeting all the design feasibility requirements. Tip mass is necessary to be placed at the wing tip to further reduce the eigen frequencies of the wing – especially the first bending.

Keywords

very flexible wing, design and optimization of wing, High-Aspect-Ratio wing, Parametric modeling

1. INTRODUCTION AND MOTIVATION

Future aircraft designs will prioritize aerodynamic performance more to minimize drag, leading to lower fuel consumption and reduced carbon emissions. This can be achieved by designing wings with a higher aspect ratio [1]. Similarly, a low structural weight can be achieved by using lighter composite materials, which will help reduce the overall mass of the aircraft [2]. Technical University of Berlin is developing the so-called TU-Flex demonstrator [3] to investigate the interactions between the mechanical and aeroelastic properties of the flight of very flexible and high aspect ratio wings.
When aiming for highly efficient flight, the objective is to achieve the enhanced performance with the least possible energy consumptions. This translates into long endurance, extended range, and reduced fuel consumption. Such efficiency can be analyzed through the Breguet range equation, which connects range with aerodynamic and structural efficiency (Figure 1). Aerodynamic efficiency improves when the ratio between lift and drag is maximized. This is typically achieved through long-span wings, which increase the wing's aspect ratio. At the same time, reducing structural mass is key to lowering operational costs by decreasing fuel burn. Since structural mass depends directly on design loads, alleviating those loads enables mass reduction. A practical method to accomplish this is the use of active load-alleviation control systems, which redistribute lift during maneuvers. Flexible wings represent a promising solution, as they combine aerodynamic and structural efficiency to deliver higher overall performance. For this reason, Highly Adaptive Research Wings (HARW) are designed with longer span and lighter structures, maximizing flexibility. The benefits include improved dynamic efficiency and lower environmental impact through reduced fuel consumption. [4]
However, these advantages come with challenges: higher bending loads, reduced maneuverability, lower flutter speeds, and potential compromises in handling and flying qualities. Addressing these issues requires a multidisciplinary design optimization (MDO) approach to mitigate risks while maintaining efficiency. One additional aspect is the reduction in a wing's

doi: 10.25967/650422

natural frequency as flexibility increases. Low natural frequencies interact with flight dynamics. Consequently, flight dynamics must account for aeroelastic couplings, while dynamic aeroelastic analyses must incorporate rigid-body motions and their interactions. Patil, Hodges, and Cesnik [5] conducted research focusing on the nonlinear aeroelastic analysis of High-Altitude Long-Endurance (HALE) aircraft. Their study was grounded in a full flow analysis of a HALE aircraft. In their methodology, they employed a geometrically-exact formulation of a mixed-form beam coupled with unsteady, finite-state aerodynamics. A significant outcome of their investigation revealed that as the tip displacement increased, the natural frequency, trim solution, and flight dynamics modes undergo considerable changes. Furthermore, their findings highlighted a notable divergence: results from the stability analysis of the model using linear analysis methods were substantially different from those obtained using methods capable of accounting for the flexibility of the wings. This underscores the importance of considering wing flexibility in the accurate analysis of HALE aircraft.

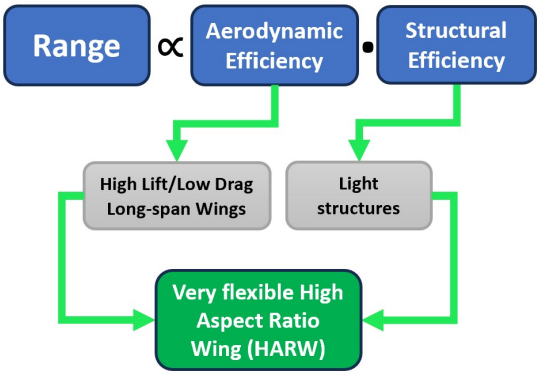

FIG 1. Relation between range, aerodynamics and structural efficiency from Bregeut range equation [4]

Similarly, the study from Su and Carlos has shown that the slender wings of highly flexible aircraft can experience large deformations even under normal operating loads. In such cases, the low-frequency elastic modes of the flexible wings often couple with the rigid-body motions of the entire aircraft [6]. As a result, the combined effects of large wing deflections, aeroelastic response, and flight dynamics must be carefully included in any nonlinear aeroelastic analysis.

Alongside aerodynamic design, advances in lightweight structures play an equally plays vital role in enabling high-performance aircraft. A clear trend in the industry has been the increased use of composite materials to reduce structural mass and fuel consumption. For instance, the Boeing 787 Dreamliner is built with about 80% composites by volume and 50% by weight [7]. More recently, new aero-structure concepts have been explored that employ lattice-based composites and discrete construction methods [8]. Furthermore, the lamination parameter based mass minimization study by Meddaiker et al. [9] concludes that optimization studies conducted on the CRM wing demonstrates that sandwich composites can achieve approximately 12% weight savings compared to current state-of-the-art monolithic composites. Furthermore, the study from Jenett et al. [10] demonstrate that employing a morphing wing in specific configurations can achieve the highest lift-to-drag ratio for a flexible wing model, making it a more effective method of generating lift than conventional ailerons. Moreover, the continuous deformation reduces form drag at low angles of attack, particularly under cruise conditions, when compared with rigid wing models. This adaptability significantly enhances overall aircraft performance by enabling the structure to adjust to different flight missions and operating conditions.

By changing the wing's structure, the stiffness and the bending loads are reduced through the passive load alleviation effect. With the same wing shape, lowering stiffness uses less structural material compared to the original design. That saved weight can be used to carry more payload or fuel [11]. On one hand, increasing the wingspan increases the wing bending loads due to the longer lever arms, on the other hand, a higher aspect ratio improves aerodynamic efficiency, hence fuel economy - as long as the structural penalties do not outweigh the aerodynamic benefits.

In recent years, several mathematical models have been developed to better understand and analyze flexible aircraft. Programs like NATASHA [12], UM/NAST [13], AEROFLEX [14], and Sharpy [15] simulate how the structure and flight dynamics interact. While some studies have validated these models, there's still not enough data to fully back them up. That's mostly because testing is expensive and uncertain [16]. Using flying demonstrators could help — they're cheaper than full-scale experiments and still provide valuable data to validate models and control systems.

Thin, swept wings with a high aspect ratio are known for their aerodynamic efficiency, which has made them a reasonable choice for future commercial aircraft designs. But with higher aspect ratios come problems like large wingtip deflections, lower flutter speeds, and reduced control authority. The Active Aeroelastic Wing (AAW) concept offers a way around these issues by combining aerodynamics, structural flexibility, and active control [17]. These wings are flexible enough to change shape during flight, making it possible to use higher aspect ratios. Multiple control surfaces help reduce bending moments at the wing roots, lower loads, cut drag, and limit elastic deformation. They also help with flutter suppression and roll control, which further improves aircraft performance [17].

This paper investigates the development of a design and optimization workflow for a highly flexible wing, with the ultimate goal of integrating it into the TU-Flex demonstrator to enable coupling analysis between structural modes and flight dynamics. In TU-Flex, the wing is intentionally designed with a low bending

frequency so that its structural dynamics interact with the aircraft's rigid-body modes. This configuration facilitates direct coupling between the wing's elastic response and the aircraft's overall rigid-body motion. Capturing this interaction is a central focus of the study, as it provides the foundation for designing and validating flight control laws tailored to highly flexible aircraft. The theoretical background and methodologies for modeling rigid–elastic coupling in such configurations are detailed in the referenced works [18]. The following chapters will first introduce the design methodology, including the modeling approach, structural assumptions, and optimization framework that guided the development of the highly flexible wing. This will be followed by a detailed discussion of the results obtained from the analyses, highlighting both the structural and aeroelastic performance of the optimized wing configuration.

2. REFERENCE AIRCRAFT WING

The Chair of Flight Mechanics, Flight Control, and Aeroelasticity at Technical University of Berlin (TU Berlin), together with the Institute of Aeroelasticity at the German Aerospace Center (DLR), have been working jointly on the development of TU-Flex test bed for aeroelastic research. The project was initiated to generate data for validating flexible aircraft (FA) and very flexible aircraft (VFA) models, while also enabling the observation and measurement of coupled interactions between aeroelastic and flight dynamics through dedicated experiments. In its initial concept, the aircraft was planned to carry two interchangeable wings. For the baseline wing, the design target was a wingtip displacement of roughly 10% of the span during maneuvers. At present, the flexible wing has been designed, optimized, fabricated, and tested for selected functionalities. A 3D Computer Added Design (CAD) representation of TU-Flex is shown in Figure 2. A more detailed description of the flexible TU-Flex wing design is provided in Gonzalez et al. [16]

FIG 2. TU-FLEX demonstrator

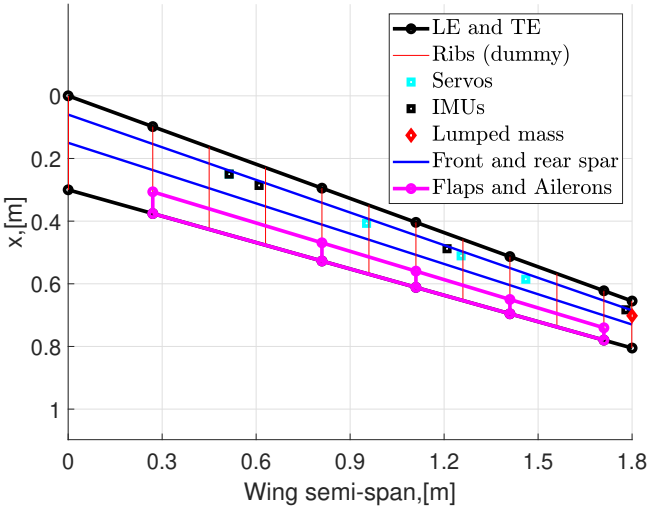

FIG 3. TU-Flex: Layout of the very flexible wing, including control surfaces, sensors, and distribution of lumped masses on the right wing

Figure 3 illustrates the topology of the TU-Flex wing, detailing the placement of the front and rear spars, as well as the location of the servos and the Inertial Measurement Unit (IMU). The control surfaces are marked in pink on the figure, with the flaps positioned inboard and the ailerons located outboard. Additionally, the figure uses a red diamond symbol to denote the positions of lumped mass, which is sued to further decrease the frequency of the wing, in case the desired frequency of the wing is not achieved after optimization. Based on the requirements, operational restrictions, and geometric constraints of the TU-Flex, Table 1 presents the main geometrical boundaries and characteristics of the conceptual system defining the TU-Flex.

TAB 1. TU-Flex conceptual requirements

Parameter	Value
Wing span, b	Max. 3.6 [m] (semi span = 1.8)
Wing mass, m	Max. 2.5 [kg]
Length, l	Max. 3 [m]
Aspect ratio, Λ	16 [-]
Sweep angle	20 [deg]
VFA mass	Max. 25 [kg]
Load Factor (min/max)	-2/4 (VFA)
Propulsion	2x Ducted fan electric-motors
Landing Gear	Tricycle retractable
Rigid-body sensors	IMU, GPS, Pitot Probe
Structural Sensors	At least 3 pairs of IMUs per wing

3. HIGHLY FLEXIBLE WING DESIGN

Wing structural design is an iterative process that requires a balance of factors such as wing mass, structural strength, structural stiffness, and aerodynamic performance. Obtaining the optimal balance of these factors is essential for the overall design of the aircraft [19, 20]. In the following subsections, the structural model, aerodynamic model, and aeroelastic modeling of TU-Flex with its highly flexible wing are described.

These components are then integrated for the optimization of the entire wing and for subsequent analyses.

3.1. Structural model

A parametric model generator ModGen [21] is used for the generation of the primary structure of the wing. This software is developed at the DLR Institute of Aeroelasticity. ModGen enables flexible parametric modeling, allowing rapid design changes and adaptations without rebuilding from scratch. This streamlines model generation and improves consistency across simulations.

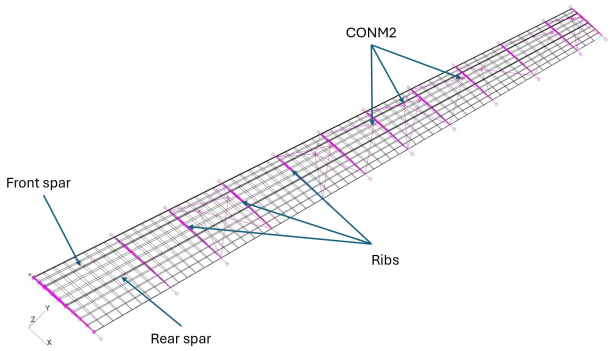

FIG 4. FE Model of the right wing along with IMUs and actuators

The Finite Element (FE) Model of the TU-Flex wing is primarily built using thin-walled composite laminates. To model the skin and spars of the wing, shell elements (CQUAD4 and CQUAD3) are used. The entire wing structure is made from the same type of glass fiber, with varying fiber orientations to satisfy specific material and performance requirements. The inner core of the wing, made of foam, is represented using solid elements (PSOLID, CHEXA and CPENTA). The CONM2 element is used to represent the masses of IMUs and actuators positioned within the Wingbox. Similarly, other concentrated masses are also included in the FE model using CONM2 cards. Wingbox consists of the front and rear spars, together with the dummy ribs. Figure 4 also illustrates the internal wing structure, with the front and rear spars positioned at 20% and 50% of the root chord length. These positions were chosen based on findings from a study conducted by González et.al. [16]

3.2. Aerodynamic model

For aerodynamic modeling, the Doublet Lattice Method (DLM) is used. This method divides the lifting surface into small trapezoidal panels also known as boxes which are arranged in columns aligned with the free-stream direction. The panel method is commonly used in aeroelastic simulations because of its balance between simplicity and accuracy, particularly when viscous effects can be neglected. [22, 23]
In this study, 10 panels are defined using the CAERO1 card in Nastran. These cards specify the layout of the trapezoidal panels. The aerodynamic model of the TU-Flex's right wing includes a total of 780 boxes. Out of the 10 panels, four control surfaces are defined using the AESURF entry.

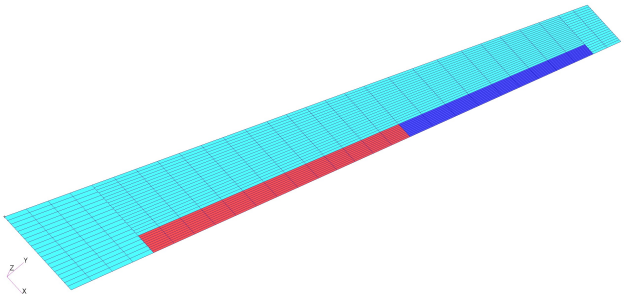

FIG 5. TU-Flex aerodynamic model with control surfaces highlighted

Figure 5 shows the aerodynamic model with the control surfaces highlighted. The red surfaces indicate the two inboard flaps (flap1 and flap2), and the blue surfaces indicate the two outboard ailerons (aileron1 and aileron2).

3.3. Aeroelastic modelling

Within aeroelastic modeling, two aspects are considered: the aero-structural coupling, which links aerodynamic forces with structural deformation, and coupling verification, which ensures the accuracy of this interaction. In general, the aerodynamic and structural surface grids do not share common grid points because their mesh densities differ. Due to this discrepancy, an interpolation method is required to accurately transfer forces and displacements between the structural and aerodynamic models. This transfer is performed using splines, which map aerodynamic forces onto the structural grid and structural displacements back onto the aerodynamic grid. [24]
To verify the accuracy of the spline model generated by MSC Flightloads [25], it is important to compare the original (unsplined) and spline-transferred values of all trim variables. For the spline model to be considered correctly implemented, these values should closely match. If any significant discrepancies arise, the spline parameters must be adjusted to better align with the numerical data.

4. LOAD ANALYSIS

There are many different types of steady and dynamic loads that can affect the design of an aircraft. These include things like gusts, vibrations at the back of the aircraft (buffet loads), pressure shocks at the engine intake (known as hammer shock), bird strikes, emergency jettisoning, landing impacts, and ground loads, among others [26]. Each of these load cases often requires a specific type of analysis, and in some cases data from physical experiments. Because of this, it's not practical to consider all of them during the early stages of aircraft design. Also, many of these loads

only affect certain parts of the aircraft. For the structural optimization of the TU-Flex wing, only a limited number of load cases that produce the highest loads are considered.

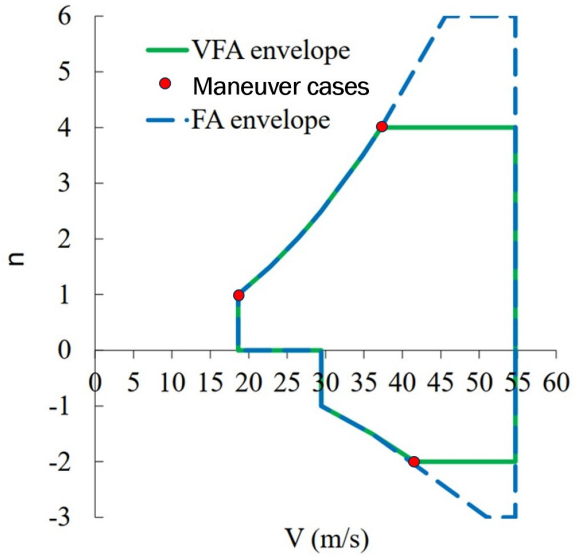

FIG 6. Flight envelope of TU-Flex with considered maneuver load cases

For the sizing of the primary structure, both maneuver and gust load are potential driving factors [27]. In this paper only the maneuver loads are considered so concerning this, a number of representative design load cases are derived from the project requirements. Figure 6 depicts the flight envelope of the TU-Flex demonstrator. The maneuver load cases include maneuvers with a positive load factor (steady straight flight) $n_z = 1g$ & (pull-up) $4g$, and negative load factor (push-down) $n_z = -2g$. These load cases are used for the sizing of the wing structure in the optimization workflow.

5. OPTIMIZATION MODEL AND WORKFLOW

5.1. Optimization model

In this section, structural sizing is carried out to evaluate and demonstrate how the different load cases obtained earlier affect the required material thickness and overall structural mass. To do this, the sizing is formulated as a structural optimization problem using MSC Nastran SOL200, with the optimization performed by IPOPT [28] – a gradient-based algorithm designed for solving large-scale nonlinear problems. The goal of structural optimization is to reduce the structural mass while meeting all required constraints. In this paper, the optimization was performed using a structural Wingbox model, along with the corresponding wing loads and allowable strain limits.

In this optimization workflow, only the right wing is subjected to sizing and optimization based on selected maneuver loads. All wing root grids are constrained to represent the wing as a cantilevered beam. This optimization is performed by computing the static aeroelastic calculations within SOL200 (with SAERO) with symmetry boundary condition. The optimization task is formally defined in Equation 1, where the design problem is expressed through mathematical formulations. In this process, the minimization of wing structural mass is selected as the objective function, while constraints ensure that design and performance requirements are satisfied.

$$min(f_{opt}(x_i)|\{g_c(x_i)\} \leq 0 \tag{1}$$

$$x_i^L \leq x_i \leq x_i^U \tag{2}$$

with:

f_{opt}	objective function,
x_i	design variable,
g_c	optimization constraint,
x_i^L, x_i^U	lower and upper bounds of the design variables

The design variables for the wing consist of the material thicknesses of the shell elements for the upper and lower skin, and spars. These variables are distributed across separate design fields, where each design field corresponds to the area between two ribs and two spars. In the optimization process, design constraints are applied to ensure that the optimizer stays within predefined limits. These constraints include both maximum wing mass, a minimum allowable thickness, aileron effectiveness of at least 1% a maximum and allowable strain for the glass fiber material.

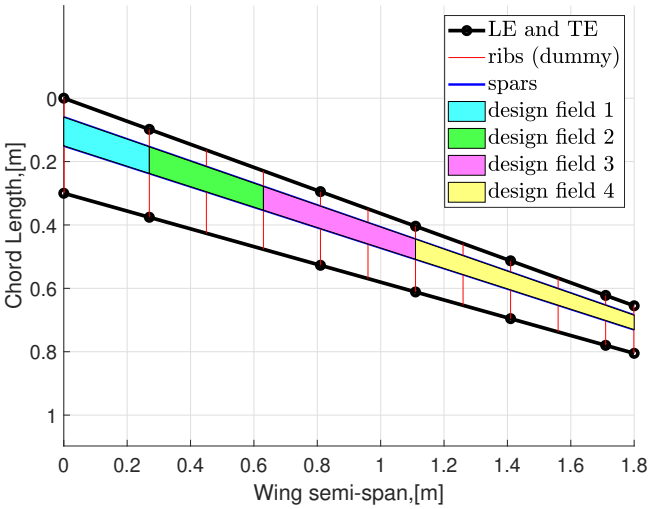

FIG 7. Design fields for skins and spars on the right wing

Specifically:

- The minimum thickness for both the upper and lower skins is set at 0.242 mm

- The minimum thickness for the spars is 0.484 mm, which is four times the minimum ply thickness of 0.121 mm

This minimum spar thickness accounts for their construction as sandwich structures, which include a foam core placed between two composite layers with different fiber orientations. The distribution of the design fields across the wing semi-span is illustrated in Figure 7. As described earlier, the region between the front and rear spars and two rib bays is defined as a single design field. Based on this definition, the TU-Flex wing was initially subdivided into 11 distinct design fields. However, manufacturing a 1.8 meter semi-wing with 11 regions of varying ply thickness introduces significant complexity, as it requires highly precise layup processes, increased tooling variations, and additional quality-control measures. Each transition between neighboring design fields must be carefully managed to avoid stress concentrations, defects, or manufacturing errors, which not only increase production time and cost but also reduce the overall robustness of the manufacturing process. To better understand the impact of design field distribution, a study by Gonzalez et al. [16] investigated the effect of varying the number of design fields on the total wing mass. Their results showed that a configuration with seven design fields provided the best compromise, achieving a lower structural mass while maintaining sufficient wingtip displacement. In addition, the study emphasized that design fields near the wingtip should maintain nearly uniform thickness.

Building on these insights, the TU-Flex design fields concept was simplified by consolidating the design fields at the wingtip. This approach not only reduces manufacturing complexity but also streamlines the optimization process. Consequently, the TU-Flex wing was finalized with only four design fields, as illustrated in Figure 7. In total, the wing has 12 design fields – with 4 each for the upper skin, lower skin, and spars – resulting in 12 design variables.

5.2. Optimization workflow

Figure 8 presents the design and optimization workflow developed for the designing and optimizing the wingbox. Once the optimization model is integrated into the workflow, the wing optimization is performed. A modal analysis is then carried out based on the optimized design, from which 10 eigenmodes are extracted. These results are visualized in Patran and discussed in Section 6.1 (Modal Analysis).

An aeroelastic analysis of the wing was also conducted to evaluate the effectiveness of the control surfaces. This analysis included aeroelastic constraints, specifically requiring a minimum of 1% effectiveness for inboard aileron 1 during optimization. If the design was found to be infeasible after optimization, adjustments were made to the material layup, material properties, geometry, or design variables to meet the required performance.

5.3. Optimization setup

Before executing the optimization task, the optimization model must be properly configured according to the project requirements. This involves defining the objective function, selecting appropriate design variables, applying relevant constraints (e.g., strain limits, thickness bounds, and mass targets), and incorporating all critical load cases and aeroelastic conditions to ensure the model reflects the intended design environment and performance goals.

The stacking sequence of the upper and lower skin as well as the front and rear spars are listed in Table 2.

TAB 2. Stacking sequence of wingbox components

Wingbox component	Stacking sequence
Upper and lower skin	$[+45, -45]^\circ$
Front and rear spar	$[-45, +45, foam, +45, -45]^\circ$

The optimization includes constraints on maximum and minimum principal strain ($\pm$10,000$\mu m/m$) in the upper and lower skins and spars under sizing load cases. The skin thickness remains fixed at 0.242 mm, while spar thickness is constrained between 0.484 mm and 1.2 cm. Additionally, the total mass of the wing is limited to 2.5 kg, which includes an extra 0.7 kg TM added to lower the wing's natural frequency. Since the optimized wing weighs about 1.95 kg, this brings the total close to the limit. The optimization starts with the maximum allowed thickness.

6. RESULTS

This section presents the results of the wing optimization. Figure 9 shows the convergence history of the wing's structural mass, comparing cases with and without a TM. Initially, the mass is 2.9 kg without and 3.6 kg with a TM, due to starting from maximum thickness values. As optimization progresses, the mass without TM drops to 1.94 kg by iteration 5, while the mass with TM decreases to about 2.45 kg by iteration 6 and then stabilizes near the upper limit.

In Figure 9, the red line indicates the project's upper mass limit of 2.5 kg per wing. The convergence of the wing mass (with TM) toward this limit demonstrates that the optimization effectively reduced mass while satisfying constraints. Figure 10 shows the spar thickness distribution along the semi-span for two cases: with and without TM, along with the upper and lower thickness bounds. The blue line represents the case without TM, starting at 0.0107 m near the root and decreasing stepwise outboard. The cyan line shows a similar trend for the case with TM, starting at 0.0104 m. The red and black horizontal lines mark the maximum and minimum spar thickness limits. This comparison highlights how the presence of a TM affects the optimized spar thickness distribution.

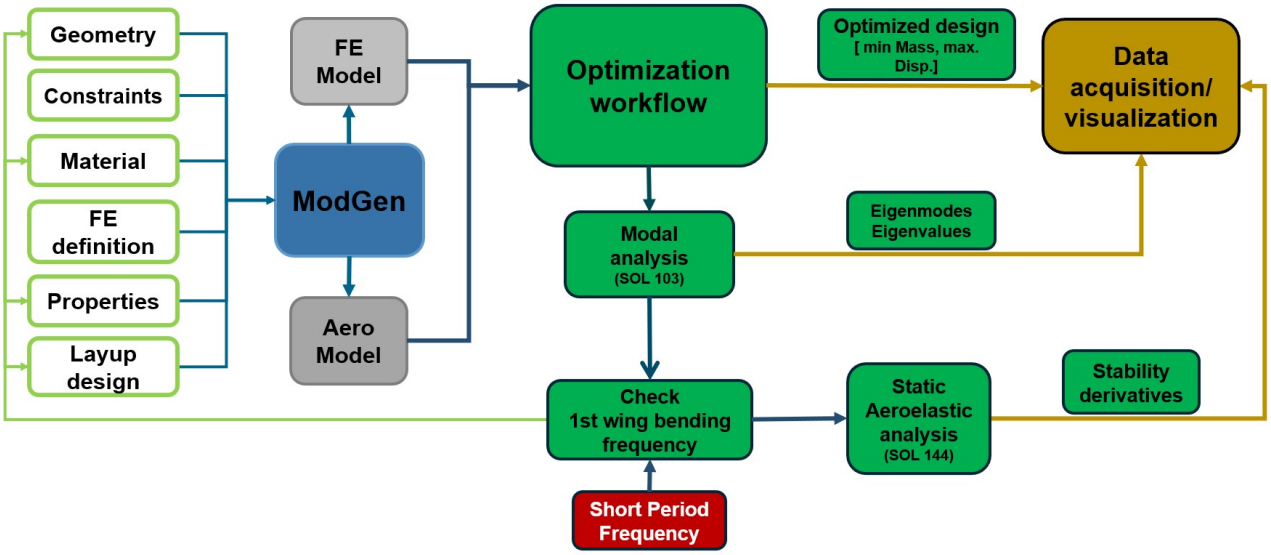

FIG 8. VF-Wing design and optimization workflow

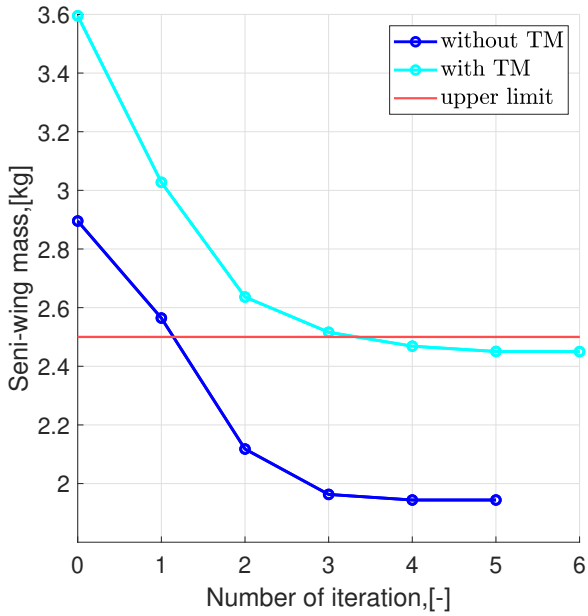

FIG 9. Convergence history of wing structural mass with and without TM

Figure 11 shows how the spar thickness in each design field changes during the optimization. At the start, all fields are set to the maximum thickness of 0.0121 m. In the left plot (without TM), the thicknesses in design fields 2, 3, and 4 gradually decrease, with field 4 showing the largest drop, reaching close to the minimum limit by the 6th iteration. Design field 1 stays almost unchanged, remaining near the upper limit. The right plot, which includes a TM, shows a similar trend. Fields 2, 3, and 4 reduce in thickness, and field 4 again drops to the minimum limit (marked by a black horizontal line). However, with the TM, the overall thicknesses are slightly lower than in the case without it. These plots show how the optimizer adjusts the thicknesses to meet structural requirements while trying to reduce weight. The steady decrease in some fields suggests that the optimizer is efficiently using less material where possible.

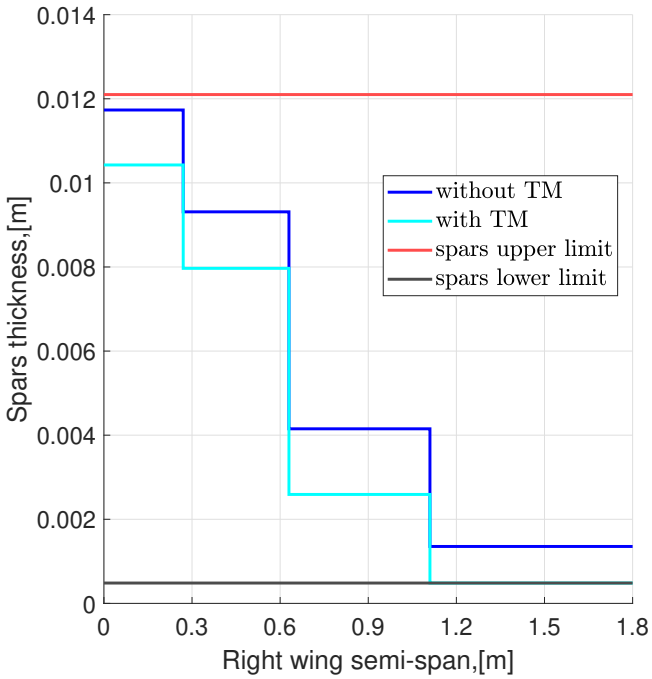

FIG 10. Spar thickness on the right wing

Figure 12 depicts the wing tip displacements under three different loading conditions (1g, 4g, and -2g). These results were visualized in Patran using the output after optimization. Table 3.6 presents a comparison between the structural optimization results of the wing spars in two configurations: with and without a tip mass. The inclusion of the TM leads to a slight reduction in wing displacement under 1g. This indicates that adding the TM decreases the overall stack thickness of the wing and therefore less stiffness. The optimized wing without the TM has a total mass of 1.94 kg, whereas the wing with the TM weighs 2.45 kg.

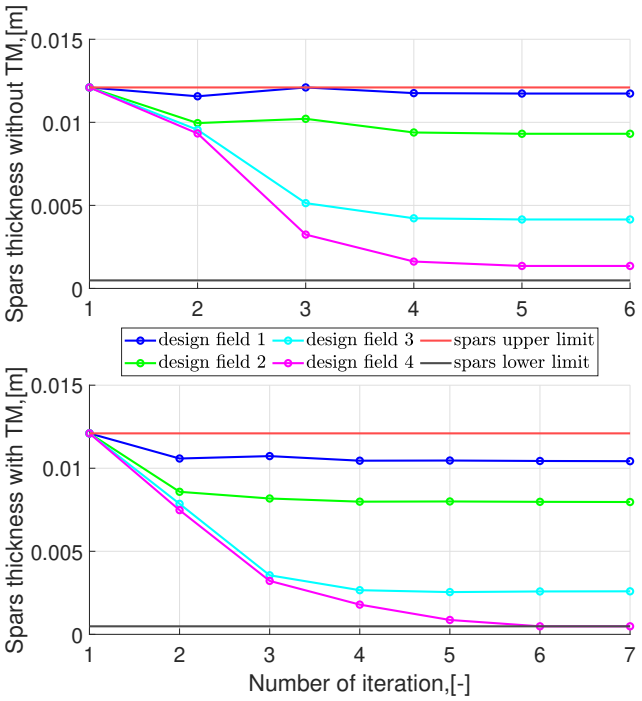

FIG 11. Convergence history of spars thickness in 4 design fields

This increase is due to the additional 0.7 kg mass added at the tip during the optimization setup aiming to reduce the eigen natural frequency of the wing. To accommodate the decreased bending loads introduced by the TM, the optimizer responds by lowering stiffness of the wing structure (in all design fields as shown in the Fig. 11). The added mass at the wing tip reduces the bending moment along the span, requiring less material in all regions to maintain structural integrity. As a result, the optimizer lowers the spar thickness across all design fields. This structural adjustment contributes to the overall reduction in mass while ensuring the wing remains within allowable strain.

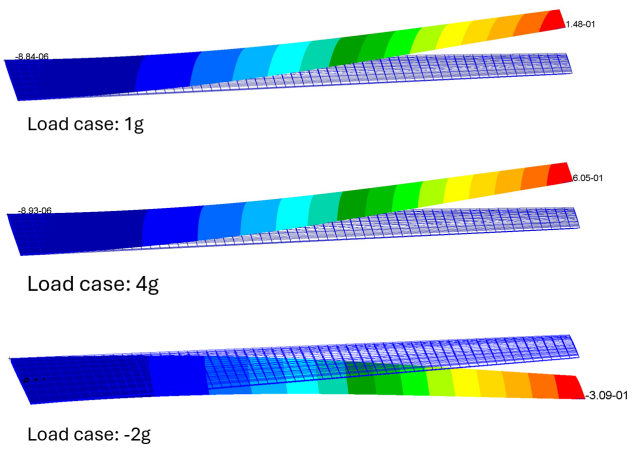

FIG 12. Wing tip displacement at different load cases

TAB 3. Results after optimization

Results	without TM	with TM
Tip displacement @ 1g [%]	8.85	8.05
Right wing mass [kg]	1.94	2.45

Figures 13 show a Von-Mises strain distribution on the upper and lower skins of the optimized wing during 4g trim maneuver. In the upper skin, the strain peaks at $8.25 \cdot 10^{-}3$, located at the wing root, highlighted by a strong red area. This high strain concentration points to potential weak spots that may be prone to failure. The colors transition smoothly from red through orange, yellow, green, to blue, illustrating a gradual decrease in strain away from the root. Overall, the strain is highest near the wing root, indicating this area experiences the most stress during the maneuver and could significantly affect the wing's structural performance. Von-Mises strain distribution across the upper and lower skins under +4g load case reveals critical insights into structural response behavior. Despite the use of a symmetric ±45° glass fiber layup, the upper skin consistently exhibits higher strain magnitudes, particularly near the wing root and at the upper skin. This can be attributed to the cambered geometry of the airfoil, which shifts the neutral axis toward the lower skin and concentrates bending deformation in the upper regions. Furthermore, localized strain amplification at the leading edge highlights the influence of curvature. While the von-Mises strain scales roughly linearly with g-load [29], the persistent location of strain hotspots across both loading directions suggests the presence of structurally sensitive zones.

However, since these strains are after optimizing the Wingbox means that the wing will held the desired maneuver loads and strains values are still in tolerable regime. This strain hotspots also suggest that there is change in thickness of the spar which can also be visualized in figure 11. In this figure, the third design field thins abruptly near one-third of the wingspan, creating a strain hotspot at its onset. Thinner structural sections in a region of high bending moment or aerodynamic load tend to concentrate strain, especially when material stiffness, thickness taper, or geometry change abruptly. This behaviour is consistent with findings in studies of wing structure under load. For example, Sinha, Klimmek, Schulze et al. [30] show in Loads analysis and structural optimization of a high aspect ratio, composite wing aircraft how skin and internal spar thicknesses play a major role in stress concentrations under manoeuvre loads. The bending moment decreases continuously towards the wing tip, but the skin thickness decrease in steps. Thus, for every design field, the bending moment is highest at the beginning (root side), therefore also the highest strains.

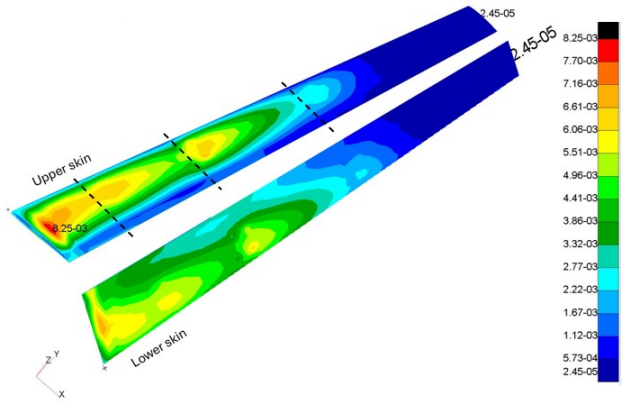

FIG 13. Strain distribution on the upper and lower skin at 4g

6.1. Modal analysis

Modal analysis, a key part of dynamic analysis, identifies a structure's natural frequencies and mode shapes. These inherent properties, determined by the structure's material, geometry, and boundary conditions, dictate how it will respond to dynamic loads. [24] In this work, Nastran SOL103 is used to perform the modal analysis. The figures from 14 to 17 show the first four eigenmodes of the wing without and with a TM at the wingtip. In both cases, the first eigenmode corresponds to the first out-of-plane wing bending mode. Differences appear in the higher modes: without the TM, the second eigenmode is the second out-of-plane bending mode, whereas with the TM, the second eigenmode is the first in-plane wing bending mode. Notably, this in-plane bending mode appears as the third eigenmode when the TM is absent. The remaining modes primarily represent wing bending.

Similarly, Table 4 presents the eigenfrequencies of the wing with and without the TM. It clearly shows that the addition of the TM causes a significant decrease in the lower natural frequencies, especially the first three eigenfrequencies, which drops drastically. This notable effect of the TM is its impact on the first eigenmode frequency, which measures the wing's natural eigen frequency. Without the TM, the first mode occurs at 4.84 Hz, but with the TM, it drops sharply to 2.07 Hz, marking a 58% decrease. This reduction shows that the wing becomes more prone to low-frequency oscillations, which can affect the aircraft's dynamic response, particularly in turbulent or gusty conditions. Thus, these effects must be carefully evaluated when balancing mass, stiffness, and the coupling between structural and flight mechanical modes of the wing. These interactions are examined in detail in the aeroelastic analysis [18].

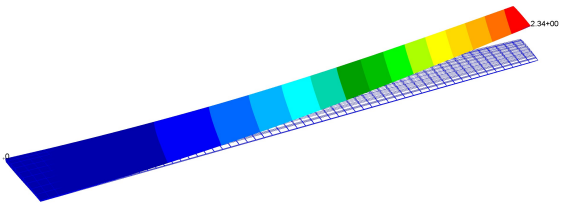

FIG 14. Mode 1 of the wing without TM: 4.84 Hz

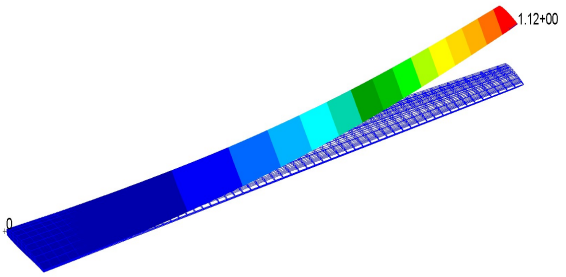

FIG 15. Mode 1 of the wing with TM: 2.07 Hz

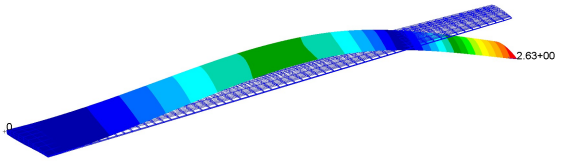

FIG 16. Mode 2 of the wing without TM: 18.21 Hz

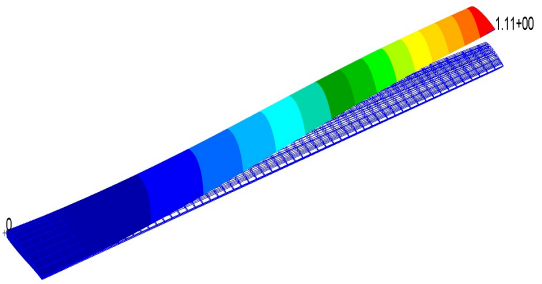

FIG 17. Mode 2 of the wing with TM: 12.32 Hz

TAB 4. First five frequencies of the VFW, with and without TM

Mode	Frequency [Hz]	
	Without TM	With TM
1	4.84	2.07
2	18.21	12.32
3	27.69	13.29
4	42.55	35.67
5	81.58	72.59

6.2. Control surface effectiveness

Aileron reversal is a type of control surface reversal that affects an aircraft's controllability. It happens when the force exerted by the aileron reverses as the aircraft reaches certain speeds. If the wing isn't

stiff enough, the aileron's movement twists the wing, altering the angle of attack and reducing lift instead of increasing it. [31]
Aileron effectiveness issues typically arise at high dynamic pressures, so an airspeed of 60 m/s is considered for analysis. The altitude is set to sea level for the simplification of the analysis. The resulting parameters for this flight condition are detailed in Table 5.
The effectiveness of the control was added as a design constraint in the optimization process to ensure that the controls have sufficient authority throughout the entire flight envelope. The effectiveness of the aileron is defined as the ratio between the roll derivative due to the deflection of the aileron of the elastic aircraft and that of the rigid aircraft and can be calculated from Equation 3 [32]

TAB 5. Parameters of aileron effectiveness calculation on TU-Flex

Parameter	Value
Mach number, Ma	0.1749
Air density, ρ	1.225 kg/m^3
Dynamic pressure, q	2205 Pa

$$\frac{C_{l\xi(elastic)}}{C_{l\xi(rigid)}} > 0 \tag{3}$$

Control effectiveness values for Ailerons 1 and 2 were taken from MSC Nastran (SOL144) results. Aileron 1 must maintain at least 1% effectiveness, while Aileron 2 can have negative effectiveness. If reversal still persists after structural optimization, a change in the wing design is necessary.

TAB 6. Ailerons effectiveness of the VFW, with and without TM

Ailerons	VFW without TM	VFW with TM
Aileron 1	20.27%	15.45%
Aileron 2	-9.38%	-14.7%

Table 3.9 shows that adding a TM reduces Aileron 1 effectiveness from 20.27% to 15.45%, and Aileron 2's effectiveness decreases from –9.38% to –14.7%, indicating that it is already in reversal, and the TM further intensifies this effect. Overall, adding the TM lowers aileron effectiveness by about 5% in both cases.

7. EVALUATION AND CONCLUSION

The wing's geometry model was developed using ModGen. Following this, the wing was optimized using the developed model and framework. Aircraft wing structures experience significant stresses and strains under design load scenarios, which affect the structural mass. However, it is not practical to consider all load cases at the early stage of the analysis. Similarly, many of these loads only affect certain parts of the aircraft. Because of this reason, only a few maneuver load cases are selected for the sizing of the structure.
The investigations conducted during the design process aim to provide insights into the advantages of parametric modeling and optimization for the TU-Flex demonstrator during the preliminary design using only the critical load cases. These analyses encompass a range of disciplines, including load analysis, aeroelasticity, aerodynamics, structural optimization, and flight mechanics. Throughout these investigations, several key aspects have emerged, highlighting their significance in the design process:

- Since the skins and spars near the wing tip are already at their minimum thickness, the flexibility to optimize and adjust the wing stiffness is mainly concentrated around the root section.
- A TM is required to lower the bending frequency in order to achieve the desired aeroelastic–flight dynamic coupling at the target flight condition.
- The control surface effectiveness results show that while Aileron 1 can still support roll control near the flight envelope limit, Aileron 2 is already in reversal, And the addition of the tip mass further degrades its performance. Overall, the TM reduces aileron effectiveness by about 5% for both surfaces.

8. OUTLOOK

In the next phase, a detailed analysis of the designed and optimized wing will be conducted. This will include a stacking sequence optimization [33] to generate manufacturable laminates tailored to the selected Wingbox geometry. The design of the wing-to-fuselage attachment will also be refined and incorporated into the wing's finite element (FE) model. To meet manufacturability requirements, the wing spars will be redesigned with additional reinforcement at the root section. In particular, spar caps will be introduced at the wing root and integrated into the optimization framework, which will require a subsequent re-optimization of the overall design. Finally, extending the wing in the spanwise direction will be investigated as a strategy to further lower the natural frequency, potentially removing the need for a TM.

Contact address:

hikmat.shahi@dlr.de, p.gonzalez.ramirez@tu-berlin.de, Wolf.krueger@dlr.de, flavio.silvestre@tu-berlin.de

References

[1] J. R. R. A. Martins, G. Kennedy, and G. K. Kenway. High aspect ratio wing design: Optimal aerostructural tradeoffs for the next generation of materials. In *52nd Aerospace Sciences Meeting, AIAA SciTech Forum*. AIAA, 2014. DOI: 10.2514/6.2014-0596.

[2] U. Kling, D. Empl, O. Boegler, and A. T. Isikveren. Future aircraft wing structures using renewable materials. In *DLRK 2015*, 2015. DocumentID: 370118.

[3] P.J. González, G. Stavorinus, H. Shahi, Y. M. Meddaikar, S. Cumnuantip, A. Voß, T. Klimmek, W. R. Krüger, and F. J. Silvestre. A preliminary structural design of a flexible flying demonstrator. In *33rd Congress of the International Council of the Aeronautical Sciences (ICAS)*, Stockholm, Sweden, Sept. 2022. International Council of the Aeronautical Sciences (ICAS).

[4] C. E. S. Cesnik, M. Ritter, J. Hilger, and C. Riso. Modeling Challenges and Opportunities for Aircraft with High-Aspect-Ratio Wings (HARW); Session 1: Aeroelastic modelling. *AR20+: Workshop on High Aspect Ratio Wing Technologies*, 2023. DOI: 10.52843/cassyni.70bjfs.

[5] M. J. Patil, D. H. Hodges, and C. E. S. Cesnik. Nonlinear aeroelasticity and flight dynamics of high-altitude long-endurance aircraft. *Journal of Aircraft*, 38(1):88–94, 2001. DOI: 10.2514/2.2738.

[6] W. Su and C. E. S. Cesnik. Dynamic response of highly flexible flying wings. *AIAA Journal*, 49(2):324–339, 2011. DOI: 10.2514/1.J050496.

[7] A. Labidi. Boeing 787 dreamliner represents composites revolution, March 2020.

[8] D. Morton, A. Xu, A. Matute, and R. F. Shepherd. Autonomous material composite morphing wing. *Journal of Composite Materials*, 57(4):711–720, Jan. 2023. ISSN: 1530-793X. DOI: 10.1177/00219983231151397.

[9] Yasser M. Meddaikar, Johannes K. S. Dillinger, Gustavo H. C. Silva, and Roeland De Breuker. Lamination-parameter-based mass minimization of the common research model wing using sandwich composites. *Journal of Aircraft*, 0(0):1–15, 2025. DOI: 10.2514/1.C037863.

[10] B. Jenett, S. Calisch, D. Cellucci, N. Cramer, N. Gershenfeld, S. Swei, and K. C. Cheung. Digital morphing wing: Active wing shaping concept using composite lattice-based cellular structures. *Soft Robotics*, 4(1):33–48, 2017. DOI: 10.1089/soro.2016.0032.

[11] P. Stahl, F.-M. Sendner, C. Rößler, M. Hornung, and A. Hermanutz. Mission and Aircraft Design of FLEXOP Unmanned Flying Demonstrator to Test Flutter Suppression within Visual Line of Sight. *17th AIAA Aviation Technology, Integration, and Operations Conference*, June 2017. DOI: 10.2514/6.2017-3766.

[12] M. J. Patil and D. H. Hodges. Flight dynamics of highly flexible flying wings. *Journal of Aircraft*, 43(6):1790–1799, 2006. DOI: 10.2514/1.17640.

[13] C. M. Shearer and C. E. S. Cesnik. Nonlinear flight dynamics of very flexible aircraft. *Journal of Aircraft*, 44(5):1528–1545, 2007. DOI: 10.2514/6.2005-5805.

[14] F. Ribeiro, P. Paglione, R. G. A. da Silva, and M. S. de Sousa. Aeroflex: a toolbox for studying the flight dynamics of highly flexible airplanes. In *Proceedings of the VII Congresso Nacional de Engenharia Mecânica*, Sao Luis, Maranhao, Brazil, 2012. ABCM.

[15] R. J. S. Simpson, R. Palacios, H. Hesse, and P. Goulart. Predictive control for alleviation of gust loads on very flexible aircraft. In *Proceedings of AIAA SciTech Forum*, AIAA 2014-0843, National Harbor, Maryland, 2014. AIAA. DOI: 10.2514/6.2014-0843.

[16] P. J. González, H. Shahi, M. Y. Meddaikar, W. R. Krüger, and F. J. Silvestre. Flexible-Wing Design Process for TU-FLEX Demonstrator. In *Proceedings of the 19th International Forum on Aeroelasticity and Structural Dynamics (IFASD 2022)*, Madrid, Spain, June 2022. International Forum on Aeroelasticity and Structural Dynamics. ISBN: 978-840942353-8. 13–17 June 2022.

[17] W. Zhao and R. K. Kapania. Static Aeroelastic Optimization of Aircraft Wing with Multiple Surfaces. In *18th AIAA/ISSMO Multidisciplinary Analysis and Optimization Conference*, Denver, Colorado, 2017. AIAA AVIATION Forum. DOI: 10.2514/6.2017-4320.

[18] P. J. González, H. Shahi, A. G. Quesada, W. R. Krüger, and F. J. Silvestre. Analysis of coupling between structural and flight mechanical modes of a flying demonstrator with highly flexible, high-aspect-ratio wing. To be published, DLRK 2025, Augsburg, 2025.

[19] M.R. Allyn and T. T. Takahashi. Conceptualizing Active Load Alleviation: Impacts on Transport Category Aircraft Wing Structural Design. 13-17 june 2016. DOI: DOI: 10.2514/6.2016-3744.

[20] T. Chen, M. Xu, and L. Xie. Aeroelastic modeling using geometrically nonlinear solid-shell elements. *Journal of Aircraft*, 52(9):2014–2024, 2014. DOI: 10.2514/1.J052765.

[21] T. Klimmek, M. Schulze, M. Abu-Zurayk, C. Ilic, and A. Merle. cpacs-mona – an independent and high-fidelity mdo-integrated process for the structural and aeroelastic design of aircraft configurations. In *International Forum on Aeroelasticity and Structural Dynamics 2019 (IFASD 2019)*, June 2019.

[22] W. P. Rodden, J. P. Giesing, and T. P. Kalman. New developments and applications of the subsonic doublet-lattice method for nonplanar configurations. In *AGARD Conference Proceedings*, CP-80-71, Part II, No. 4, Cambridge, UK, 1971. AGARD.

[23] W. P. Rodden, P. F. Taylor, and S. C. McIntosh Jr. Further refinement of the subsonic doublet-lattice method. *Journal of Aircraft*, 35(5):720–727, 1998. DOI: 10.2514/2.2364.

[24] MSC Software Corporation. *MSC Nastran Design and Optimization User's Guide*. Hexagon MSC Software, Newport Beach, CA, 2025. Version 2025, accessed via institutional license.

[25] MSC Software Corporation. *MSC FlightLoads 2024 User Guide*. Hexagon AB, Newport Beach, CA, USA, 2024. Software documentation.

[26] W. G. Luber, J. Becker, and O. Sensburg. The impact of dynamic loads on the design of military aircraft. In *Proceedings of the AGARD Conference*, Florence, Italy, 1996. AGARD.

[27] A. Voß and T. Klimmek. Parametric aeroelastic modeling, maneuver loads analysis using CFD methods and structural design of a fighter aircraft. Standard, Aerospace Science and Technology, Nov. 2022. URL: https://elib.dlr.de/194183/1/Vo

[28] A. Wächter and L. T. Biegler. On the implementation of an interior-point filter line-search algorithm for large-scale nonlinear programming. *Mathematical Programming*, 106(1):25–57, 2006. ISSN: 1436-4646. DOI: 10.1007/s10107-004-0559-y.

[29] P. Dümig. Transformation of in-flight measured loads to a fatigue test spectrum. Master's thesis, Dalarna University, Sweden, 2022. Thesis; real in-flight measured loads; uses von-Mises strain / stress related to load factor n_z.

[30] Kautuk Sinha, Thomas Klimmek, Matthias Schulze, and Vega Handojo. Loads analysis and structural optimization of a high aspect ratio, composite wing aircraft. *CEAS Aeronautical Journal*, 12(1):233–243, 2021. DOI: 10.1007/s13272-021-00494-x.

[31] R. L. Bisplinghoff, H. Ashley, and R. L. Halfman. *Aeroelasticity*. Dover Publications, Mineola, New York, dover edition edition, 1996. ISBN: 978-0486691861.

[32] V. Handojo. Contribution to load alleviation in aircraft pre-design and its influence on structural mass and fatigue, 2020. [Retrieved: 07.01.2024]. https://elib.dlr.de/139558/1/DLR-FB-2020-47.pdf.

[33] Y. M. Meddaikar, F. X. Irisarri, and M. M. Abdalla. Laminate optimization of blended composite structures using a modified shepard's method and stacking sequence tables. *Structural and Multidisciplinary Optimization*, 55(2):535–546, 2017. DOI: 10.1007/s00158-016-1508-0.